

## High pressure range of the addition of HO to HO, NO, NO<sub>2</sub>, and CO. I. Saturated laser induced fluorescence measurements at 298 K

R. Forster, M. Frost, D. Fulle, H. F. Hamann, H. Hippler et al.

Citation: *J. Chem. Phys.* **103**, 2949 (1995); doi: 10.1063/1.470482

View online: <http://dx.doi.org/10.1063/1.470482>

View Table of Contents: <http://jcp.aip.org/resource/1/JCPSA6/v103/i8>

Published by the [AIP Publishing LLC](http://www.aip.org).

---

### Additional information on *J. Chem. Phys.*

Journal Homepage: <http://jcp.aip.org/>

Journal Information: [http://jcp.aip.org/about/about\\_the\\_journal](http://jcp.aip.org/about/about_the_journal)

Top downloads: [http://jcp.aip.org/features/most\\_downloaded](http://jcp.aip.org/features/most_downloaded)

Information for Authors: <http://jcp.aip.org/authors>

## ADVERTISEMENT



Explore the **Most Cited**  
Collection in Applied Physics

**AIP**  
Publishing

# High pressure range of the addition of HO to HO, NO, NO<sub>2</sub>, and CO.

## I. Saturated laser induced fluorescence measurements at 298 K

R. Forster, M. Frost, D. Fulle, H. F. Hamann, H. Hippler,<sup>a)</sup> A. Schlegel, and J. Troe  
*Institut für Physikalische Chemie, Universität Göttingen, Tammannstrasse 6, D-37077 Göttingen, Germany*

(Received 28 March 1995; accepted 18 May 1995)

Saturated laser induced fluorescence is used for the sensitive detection of radicals in high pressure gases. The method and its application to a series of addition reactions of HO radicals in the high pressure regime are described. Experiments between 1 and 150 bar of the bath gas He allow for falloff extrapolations to the high pressure limit of the recombination reactions. Limiting rate constants (in cm<sup>3</sup> molecule<sup>-1</sup> s<sup>-1</sup>) of  $2.2 \times 10^{-11}$  for HO+HO→H<sub>2</sub>O<sub>2</sub>, of  $3.3 \times 10^{-11}$  for HO+NO→HONO, of  $7.5 \times 10^{-11}$  for HO+NO<sub>2</sub>→HONO<sub>2</sub>, and of  $9.7 \times 10^{-13}$  for HO+CO→HOCO (and H+CO<sub>2</sub>) are derived at 298 K. © 1995 American Institute of Physics.

### I. INTRODUCTION

The high pressure limit of unimolecular bond fission and the reverse radical recombination reactions is closely related to the properties of potential energy surfaces at large bond extensions. Although it is not possible to derive particularly detailed information on the potential from the measured rate constants, a global picture of the potential or at least a check of potential energy calculations can be obtained (see, e.g. Refs. 1–3). It is therefore highly desirable to extend falloff curves of the reactions to the high pressure limit. Measurements of this type are also required to construct reliable and complete representations of dissociation and recombination rate constants over the full falloff range such as required in atmospheric and combustion chemistry.<sup>4,5</sup>

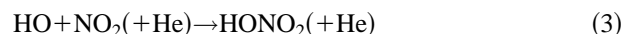
In order to approach the high pressure limit sufficiently closely for reactions between small species, pressures above 1 bar or even much higher have to be applied. Therefore, one is looking for sensitive detection methods for the reactants in high pressure gases. While we have used uv or visible absorption measurements in previous studies of this type (see, e.g., Refs. 6–8), in the present work we investigated the possibilities of employing laser induced fluorescence (LIF) in high pressure environments. Often, LIF is recorded under conditions where the signal is influenced by collisional quenching of the emitting electronically excited states. Clearly this would complicate high pressure measurements. One might think of using LIF from strongly predissociated levels which, however, would reduce the detection sensitivity. In the present work instead we investigated the possibilities of employing LIF under saturation conditions (SLIF) from unpredissociated levels. As shown below, this method works remarkably well and provides the required sensitive detection for a class of otherwise not easily accessible reactions.

The present article describes the first set of observations up to bath gas pressures of 150 bar for a set of HO radical addition reactions. HO reactions continue to be of central interest in atmospheric and combustion chemistry<sup>4,5,9</sup> such

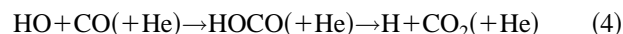
that the studied reactions are also of considerable practical relevance. At first, we study the HO self-reaction



which is in close connection with the H<sub>2</sub>O<sub>2</sub> dissociation under thermal and under isolated molecule conditions.<sup>10</sup> Our measurements of the complete falloff curve allow for an unambiguous solution of earlier difficulties<sup>11,12</sup> to separate low pressure rates of reaction (1) from rates of the competing reaction HO+HO→H<sub>2</sub>O+O, see below. The usefulness of high pressure measurements even for low pressure problems here becomes particularly evident. By adding other reactants in excess to HO, besides reaction (1) the addition processes



were studied up to the high pressure limit as well. Finally, the complex-forming bimolecular reaction



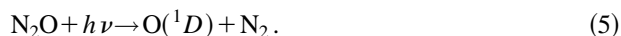
was investigated near room temperature. As this reaction showed a weak pressure dependence at pressures below 1 bar (see summary in Refs. 4, 5, and 9), it appeared of great interest to see how far an increase of the apparent second order rate constant with increasing pressure would go. A more detailed investigation of reaction (4) over wide ranges of temperature and pressure will be given in part II of this series.<sup>13</sup> A theoretical analysis of the falloff curves of reactions (1)–(3) together with measurements over wider temperature ranges will be described later; other studies of HO addition reactions in the high pressure range follow as well.

### II. EXPERIMENTAL TECHNIQUE

Our experiments employed the pump and probe technique. HO radicals were produced through laser flash photolysis of appropriate precursor mixtures. Fluorescence of HO after a given time delay then was induced by the pulse of a probe laser and recorded. By varying the time delay between the pump and probe pulses, concentration-time profiles of HO were obtained by monitoring the fluorescence intensity.

<sup>a)</sup>Institut für Physikalische Chemie und Elektrochemie, Universität Karlsruhe, Kaiserstrasse 12, D-76128 Karlsruhe, Germany.

Due to the long mixing times of the employed high pressure reaction mixtures, the precursor molecules had to be sufficiently stable. In general we worked with reaction mixtures of N<sub>2</sub>O (3–40 mbar), H<sub>2</sub>O (20 mbar), and He (1–150 bar). Suitable amounts of other reactants like NO or CO then were added. N<sub>2</sub>O was photolyzed at 193 nm where, with a quantum yield of unity and an absorption cross section of  $9.0 \times 10^{-20}$  cm<sup>2</sup> molecule<sup>-1</sup>, O(<sup>1</sup>D) atoms are formed through



The O(<sup>1</sup>D) atoms subsequently react with H<sub>2</sub>O to form HO via



with a rate constant  $k_6 = 2.2 \times 10^{-10}$  cm<sup>3</sup> molecule<sup>-1</sup> s<sup>-1</sup>.<sup>4</sup> N<sub>2</sub>O/H<sub>2</sub>O/NO<sub>2</sub> mixtures turned out not to be sufficiently stable. Therefore, HO was also prepared by flash photolysis of HNO<sub>3</sub> at 248 nm via



(quantum yield of unity, absorption cross section =  $2.0 \times 10^{-20}$  cm<sup>2</sup> molecule<sup>-1</sup>, Ref. 4). In this case the reaction mixtures contained HNO<sub>3</sub>, NO<sub>2</sub>, and He.

N<sub>2</sub>O, NO, NO<sub>2</sub>, CO, He, and O<sub>2</sub> (from Messer Griesheim, purities of >99.99%, 99.5%, 98%, 99.97%, 99.996%, and 99.995%, respectively) were used without further purification. H<sub>2</sub>O was demineralized and degassed. HNO<sub>3</sub> was distilled from a solution of 1:3 ppv of HNO<sub>3</sub> and H<sub>2</sub>SO<sub>4</sub> (both suprapure grade) and collected at 77 K. The distillate was degassed and the middle fraction used.

The reaction mixtures were made up either in an 8 ℓ aluminum cylinder sealed by PTFE O rings or a 40 ℓ stainless steel vessel for high purity gases (Messer Griesheim). Solenoid valves (Nova Swiss) allowed these gases to be introduced into and expelled from the reaction cell. Thus at high pressures a refilling system was established to prevent the depletion of HO precursors and the accumulation of reaction products in the cell. At pressures below 8 bar, the reaction mixtures were flown directly through the cell. Pressures were measured with a series of pressure gauges [Okhura Electronics (>9 bar), Setra (0.1–8 bar), MKS Baratron (<0.1 bar)].

The high pressure reaction cell was fabricated from a stainless steel cylinder of 7 cm length and 12 cm diameter. It was closed by two sets of perpendicularly arranged quartz windows (Suprasil grade A) of 35 mm diameter and 20 mm thickness and sealed by PTFE O rings. In this way two perpendicular optical paths of 4 cm length were produced which overlapped over 2 cm at the center of the reaction cell.

The photolysis excimer laser (Lambda Physik EMG 102) was operated either at 193 nm (ArF, 150 mJ, 17 ns) or at 248 nm (KrF, 250 mJ, 20 ns). For HO detection, an excimer laser (Lambda Physik EMG 200) was operated at 308 nm (XeCl, 500 mJ, 25 ns), pumping a dye laser (Lambda Physik FL 3002, sulforhodamine B) whose output was frequency doubled in a BBO crystal (>3 mJ, 14 ns) and tuned to the Q<sub>1</sub>(2) line (307.995 nm) of the A <sup>2</sup>Σ<sup>+</sup> (v' = 0) ← X <sup>2</sup>Π (v'' = 0) band of the HO radical. Fluores-

cence light was collected into a monochromator (Jobin Yvon HL, grating blazed at 300 nm, aperture = f/2, operating resolution 16 nm), the detector being placed perpendicular to the counterpropagating pump and probe pulses. The monochromator was tuned off resonance of the excitation wavelength levels of the (0,0) band. The detector was a photomultiplier (EMI 9813 QGB).

The data acquisition system as well as the solenoid valves, controlling the gas handling, were connected to a personal computer. The delays between photolysis and probe laser pulses were produced by a delay generator (SRS DG 535) and controlled by an IEEE-488 port. For each delay, the output of the photomultiplier was amplified (LeCroy 133B), integrated over a 50–90 ns gate width (SRS SR 250), digitized, stored, and further handled by the computer. All decay profiles were fitted using nonlinear least square fitting procedures employing a Marquardt–Levenberg algorithm for χ<sup>2</sup> minimization. In general, equal decay constants were found on changing from a three-parameter (amplitude, decay constant, background intensity) to a two parameter fit (amplitude, decay constant) when equal prephotolysis and decay background signals were assumed. Diffusional loss of HO from the detection volume as well as reactions of HO with photolysis precursors were negligible in all cases. In order to study reaction (1), the photolysis laser fluence had to be measured by an energy gauge (Gentec). The beam was restricted to nearly spherical shape (diameter 3 mm) and the intensity profile was carefully recorded.

### III. LASER SATURATED INDUCED FLUORESCENCE

The technique of saturated laser induced fluorescence (SLIF) has been described before<sup>14–16</sup> as a method to minimize the influence of excited state collisional quenching on the observed fluorescence. The application of this technique requires sufficiently strong laser powers such that, after absorption of a photon, spontaneous emission and collisional quenching of the excited states are overrun by stimulated emission. The conditions for this technique to apply could be fulfilled in our experiments.<sup>14</sup> The quantitative correlation between observed fluorescence intensities and the concentration of the emitting species in low and medium pressure flames was established by model calculations.<sup>15,16</sup> In order to determine the limits of applicability of the technique under our high pressure conditions, the following kinetic model, describing radiational and collisional transitions, was set up.

(i) The relaxation times for rotational energy transfer in the electronically excited A <sup>2</sup>Σ<sup>+</sup> (v' = 0) state and in the electronic ground state X <sup>2</sup>Π (v'' = 0) were calculated using the rate constants for state-to-state rotational energy transfer (RET) from Ref. 17 for the A state and from Refs. 18 and 19 for the X state. Missing state-to-state rate constants for RET were either obtained through detailed balance or estimated using an exponential energy gap law. Under all of our conditions the populations of rotational levels in the electronic ground state as well as in the excited state were found to be strongly coupled due to fast RET. Within a small fraction of the duration of laser pulse (at 1 bar within 0.5 ns) thermal equilibrium between rotational states is established in the electronically excited A state and in the electronic ground

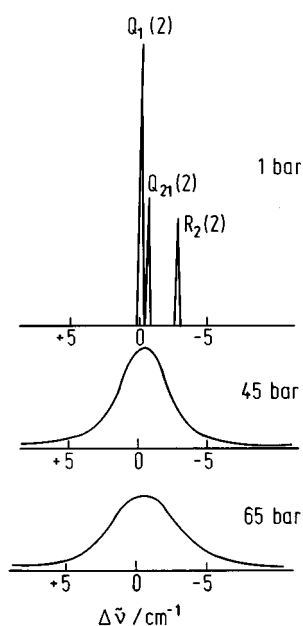
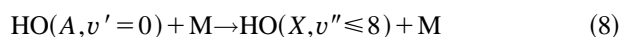


FIG. 1. Pressure broadening of the  $Q_1(2)$  line of the  $\text{HO}(A \ ^2\Sigma, v'=0) \leftarrow \text{HO}(X \ ^2\Pi, v''=0)$  transition recorded by fluorescence excitation spectroscopy (band width of the excitation laser about  $0.1 \text{ cm}^{-1}$ , bath gas He, 298 K).

state. Equilibration between the lambda doublet states of HO is similarly fast under high pressure conditions such that lambda doublet splitting effects had not further to be considered.

(ii) Absolute cross sections for absorption and stimulated emission were derived from the pressure broadened lines of the fluorescence excitation spectra (see Fig. 1) recorded in the pressure range 1–65 bar of He. At 1 bar and 298 K the observed linewidth of  $0.2 \text{ cm}^{-1}$  was attributed to a Voigt profile. Assuming a pressure independent oscillator strength of  $f_\infty = 1.1 \times 10^{-3}$  (Ref. 20) for the (0,0) band of the ( $A \leftarrow X$ ) transition, an absorption cross section at the maximum of the  $Q_1(2)$  line of  $\sigma_{\text{max}} = 2.2 \times 10^{-16} \text{ cm}^2 \text{ molecule}^{-1}$  was obtained which is in good agreement with the results from Ref. 21. For a typical laser intensity of  $2 \text{ MW/cm}^2$ , the rate for absorption and stimulated emission was calculated to be  $7 \times 10^8 \text{ s}^{-1}$  at 1 bar and 298 K. At higher pressures, the  $Q_1(2)$  line could no longer be separated from the neighboring weaker transitions  $Q_{21}(2)$  and  $R_2(2)$ . Nevertheless, maximum absorption cross sections at higher pressures could be estimated with sufficient accuracy by neglecting the weak contributions from the  $Q_{21}(2)$  and  $R_2(2)$  transition to the pressure broadened fluorescence excitation spectrum.

(iii) The intensity of spontaneous emission from electronically excited  $\text{HO}(A, v'=0)$  follows from its lifetime under collision-free conditions which is of the order of 100 ns.<sup>15</sup> Under our experimental conditions, the lifetime of  $\text{HO}(A, v'=0)$  is drastically shortened by collisional quenching



not only by the high pressure bath gas  $\text{M}=\text{He}$  but also by  $\text{M}=\text{H}_2\text{O}$ ,  $\text{N}_2\text{O}$  or added reaction partners like CO, NO, or

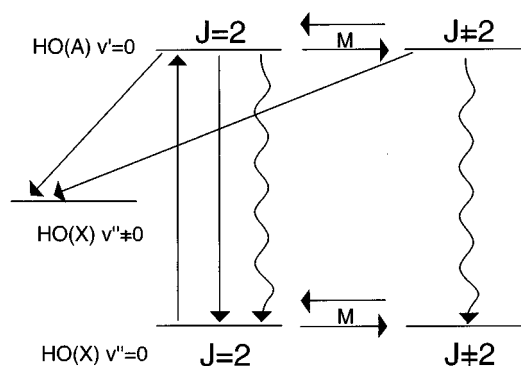


FIG. 2. Kinetic model for saturated laser induced fluorescence (SLIF) of HO used in the present work.

$\text{NO}_2$ . Consequently, spontaneous fluorescence, like stimulated emission, could only be observed during the time of laser excitation and it was monitored off resonance of the  $Q_1(2)$  transition for a better discrimination against Rayleigh scattering. Vibrational relaxation was found not to be fast enough<sup>22</sup> to repopulate  $\text{HO}(X, v''=0)$  during the fluorescence excitation pulse.

On the basis of the described input parameters, our kinetic model for SLIF was constructed. Figure 2 summarizes the included transitions. Because of its simplicity, the application of this model is limited to higher pressures ( $\geq 0.3$  bar of He). The laser pulse was represented by a rectangular pulse with constant intensity and the kinetic equations were numerically solved using an implementation of the DIFSUB routine described by Gear.<sup>23</sup> The observed dependence of the fluorescence intensity on the fluence of the LIF pump laser is in quantitative agreement with the results from this model calculation, see Fig. 3. The good performance of the described model for SLIF allowed us to perform quantitative HO concentration-time measurements under near to saturation conditions for all experiments of the present work.

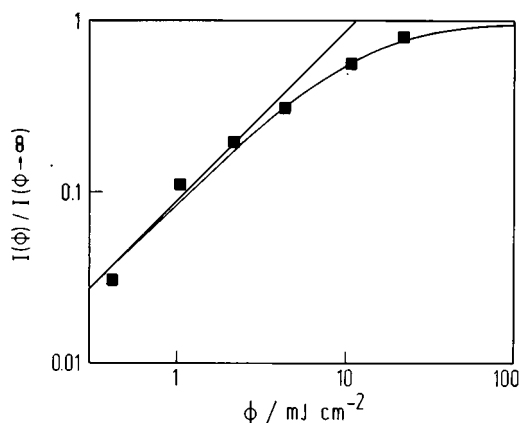
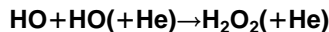


FIG. 3. Dependence of the fluorescence intensity  $I$  on the fluence  $\phi$  of the exciting laser (solid line: model calculation for 1 bar of He and 20 mbar of  $\text{H}_2\text{O}$ , see the text; points: experimental results).

## IV. RESULTS AND DISCUSSION

### A. Falloff curve of the HO self-reaction

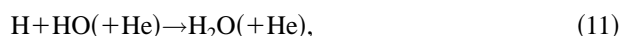


Before the addition of HO to other reactants could be studied, the self-reaction had to be investigated in detail. This reaction was always present even though often to only a small extent, such that its contribution had to be known with certainty. Besides this, the self-reaction is of great interest itself, see, Ref. 10.

Hydroxyl radicals were prepared by reactions (5) and (6) and then decayed in a second-order self-reaction with two competing reaction channels (1) and (9)



As reaction (1) occurs on a singlet H<sub>2</sub>O<sub>2</sub> potential energy surface whereas reaction (9) proceeds on a triplet surface, the two channels were assumed to be completely separated, not involving a common intermediate (see *ab initio* calculations in Refs. 24 and 25). The formation of O(<sup>3</sup>P) atoms in reaction (9) leads to further consumption of HO radicals via two subsequent reactions



where reaction (10) has a rate constant of  $k_{10} = 3.3 \times 10^{-11} \text{ cm}^3 \text{ molecule}^{-1} \text{ s}^{-1}$ .<sup>4</sup> This complication can easily be overcome if reactions (10) and (11) are suppressed by converting all O(<sup>3</sup>P) atoms into ozone through the addition of sufficiently high amounts of molecular oxygen (50–200 mbar). The rate of the reaction



is known under high pressure conditions from Ref. 26. The reaction of HO with ozone



( $k_{13} = 6.7 \times 10^{-14} \text{ cm}^3 \text{ molecule}^{-1} \text{ s}^{-1}$ , see Ref. 4) is much slower than reactions (1) and (9) such that, under our experimental conditions, HO decays in a clean second-order reaction with a rate constant  $k_{1,\text{exp}} = k_1 + k_9$ .

For the determination of the absolute value of the second-order rate constant one has to know the absolute concentration of hydroxyl radicals. A simple calculation of the initial HO concentration from the initial amount of O(<sup>1</sup>D) produced in reaction (5) is made difficult by the competition of the HO producing reaction (6) with the following loss reactions of O(<sup>1</sup>D)



with the rate constants  $k_{14} = 7.2 \times 10^{-11} \text{ cm}^3 \text{ molecule}^{-1} \text{ s}^{-1}$  and  $k_{15} = 4.4 \times 10^{-11} \text{ cm}^3 \text{ molecule}^{-1} \text{ s}^{-1}$  from Ref. 4. Reaction (16) summarizes all electronic deactivation processes of O(<sup>1</sup>D) with all possible colliders (e.g., M = N<sub>2</sub>O, H<sub>2</sub>O, O<sub>2</sub>,

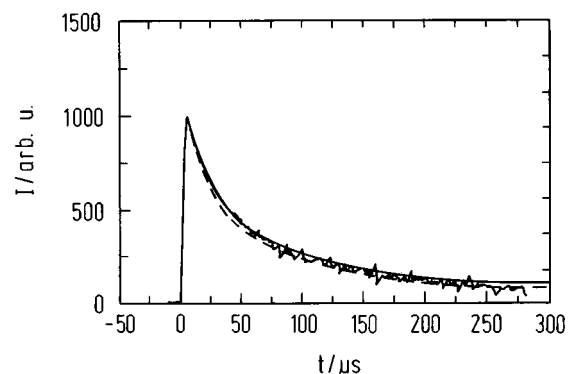


FIG. 4. HO concentration-time profile under conditions where the reaction HO+HO dominates and only small contributions from the reaction HO+NO are present (experiment at 102 bar of He, 21.6 mbar of H<sub>2</sub>O, 4.8 mbar of N<sub>2</sub>O, and 52 mbar of O<sub>2</sub>; the laser photolysis produced  $6.3 \times 10^{14} \text{ molecule cm}^{-3}$  of HO and  $5.1 \times 10^{13} \text{ molecule cm}^{-3}$  of NO; the solid line corresponds to a second-order rate law based on reactions (1) and (9) only whereas the dashed line gives the results of the kinetic simulation incorporating the complete reaction mechanism).

and He). Under our experimental conditions reactions (16) is essentially controlled by collisions of O(<sup>1</sup>D) with molecular oxygen ( $k_{14} = 4.4 \times 10^{-11} \text{ cm}^3 \text{ molecule}^{-1} \text{ s}^{-1}$ ).<sup>4</sup> The formed O(<sup>3</sup>P) atoms are removed by reaction (12). A small amount of NO is also produced by reaction (14). The subsequent reaction of NO with HO, i.e., reaction (2), can be suppressed by keeping the initial NO concentration ( $[\text{NO}]_0$ ) low compared to the initial HO concentration ( $[\text{HO}]_0$ ). In our experiments, a ratio of  $[\text{HO}]_0/[\text{NO}]_0$  between 5 and 30 was always accomplished by selecting initial concentrations of N<sub>2</sub>O and H<sub>2</sub>O such that  $[\text{H}_2\text{O}]_0/[\text{N}_2\text{O}]_0 = 1.5\text{--}9$ . However, at later times reaction (2) may compete with reactions (1) and (9), see Fig. 4. Based on these considerations, the initial HO concentrations were determined by two independent methods. First,  $[\text{HO}]_0$  was calculated from the initial concentration of electronically excited oxygen atoms,  $[\text{O}({}^1D)]_0$ , such as obtained from N<sub>2</sub>O photolysis, and the secondary yield of HO production,  $Y(\text{HO})$

$$[\text{HO}]_0 = Y(\text{HO}) \cdot [\text{O}({}^1D)]_0. \quad (17)$$

From the discussed reaction mechanism, the following expression for the HO yield  $Y(\text{HO})$  is derived

$$\frac{1}{Y(\text{HO})} = \frac{1}{2} \left( 1 + \frac{k_{16}[\text{O}_2]_0}{k_6[\text{H}_2\text{O}]_0} + \frac{(k_{14} + k_{15})[\text{N}_2\text{O}]_0}{k_6[\text{H}_2\text{O}]_0} \right) \quad (18)$$

which, under our experimental conditions, depends more sensitively on the ratio  $[\text{O}_2]_0/[\text{N}_2\text{O}]_0$  than on the ratio  $[\text{H}_2\text{O}]_0/[\text{N}_2\text{O}]_0$ . The O(<sup>1</sup>D) concentration, for weak absorption of the photolysis laser, such as it was always the case under our experimental conditions, was given by

$$[\text{O}({}^1D)] = \phi_{193\text{nm},5} \cdot \sigma_5 \cdot F_L \cdot [\text{N}_2\text{O}]_0, \quad (19)$$

where  $F_L$  is the calibrated fluence of the laser pulse. In order to maximize the production of HO radicals and at the same time to minimize the production of NO, we always prepared gas mixtures initially containing the maximum possible partial pressure of water vapor. The vapor pressure of liquid water was shown to be always established in our high pres-

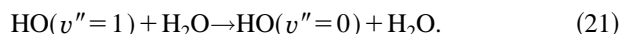
sure reaction mixtures. A second method for the determination of the initial HO concentration was applied in a separate set of experiments. Here, initially formed HO was converted into HNO<sub>3</sub> by adding sufficiently high concentrations of NO<sub>2</sub>. The total amount of HNO<sub>3</sub> produced, which was determined by uv absorption at 184 nm, agreed within 30% with the initial HO concentration derived by the first method, thus confirming the correctness of our [HO]<sub>0</sub> calibration procedure.

In order to be sure to correctly analyze this complex kinetic scheme, we have performed experiments over wide ranges of gas mixtures. The observed SLIF signals were evaluated according to the second-order rate law.

$$\frac{1}{[\text{HO}]} = \frac{1}{[\text{HO}]_0} + 2k_{1,\text{exp}}t. \quad (20)$$

The first part of the HO decay traces (where [HO] ≫ [NO]) were all well reproduced by Eq. (20). Later, when [HO] was of the order of [NO], deviations were expected. This is seen in Fig. 4 where significant deviations between clean second-order decay and the experimental data appeared only at longer times. Calculations with the kinetic model of reactions (1), (2), and (9) well reproduce the full experimental [HO] profile. The incorporation of O(<sup>3</sup>P) reactions had only negligible effects.

There is, however, an additional problem: as seen in Fig. 4, the rise of the LIF signal did not follow the short pulse of the photolysis laser. This is due to vibrational relaxation of HO(*X*, *v*"=1) radicals which are produced in reaction (6) with a yield of about 20%.<sup>27</sup> This vibrational relaxation under our conditions is dominated by collisions with water



Using the value of  $k_{21} = 1.4 \times 10^{-11} \text{ cm}^3 \text{ molecule}^{-1} \text{ s}^{-1}$  from Ref. 28, a lifetime of  $\tau = 100 \text{ ns}$  is calculated under our conditions which is in excellent agreement with our observations. Therefore, [HO] decays with Eq. (20) were evaluated only after relaxation was complete.

The self-reaction of HO radicals is assumed to proceed via two independent reaction channels (1) and (9), see above. Channel (1) corresponds to the recombination to H<sub>2</sub>O<sub>2</sub> with a normal falloff pressure dependence. Channel (9) on a triplet potential leads to H<sub>2</sub>O and O(<sup>3</sup>P). A pressure independent value of  $k_9 = 1.9 \times 10^{-12} \text{ cm}^3 \text{ molecule}^{-1} \text{ s}^{-1}$  was recommended in Ref. 4. Thus the total second-order rate constant of HO consumption should be given by the sum  $k_{1,\text{exp}} = k_1 + k_9$ , i.e., by an S-shaped transition falloff curve between two pressure independent limiting rate constants. The results of our experiments, such as given in Table I and represented in Fig. 5, correspond to this expectation.

In order to separate  $k_1$  and  $k_9$ , our results are combined with earlier literature data obtained at lower pressures. There exist only few direct kinetic studies of reaction (1).<sup>11,12,29</sup> The bath gas N<sub>2</sub> was used in Refs. 11 and 12 while SF<sub>6</sub> was employed in Ref. 29. The rate constants for N<sub>2</sub> and He do not differ too much, such their influence in the medium pressure range (above 1 bar) should be much weaker than the experi-

TABLE I. Second order rate constants for the reaction HO+HO (+He)→products ([He] in molecule cm<sup>-3</sup>,  $k_{1,\text{exp}}$  in cm<sup>3</sup> molecule<sup>-1</sup> s<sup>-1</sup>, No. = number of experiments).

[He]	$\frac{[\text{HO}]_0}{[\text{NO}]_0}$	No.	$k_{1,\text{exp}}$
3.9·10 <sup>19</sup>	32 ±2	1	(7.3±2.5)·10 <sup>-12</sup>
5.3·10 <sup>19</sup>	20 ±1	1	(8.1±2.8)·10 <sup>-12</sup>
6.3·10 <sup>19</sup>	22 ±1	2	(7.8±2.7)·10 <sup>-12</sup>
8.0·10 <sup>19</sup>	18 ±1	1	(1.1±0.4)·10 <sup>-11</sup>
1.1·10 <sup>20</sup>	19 ±1	2	(1.2±0.4)·10 <sup>-11</sup>
1.2·10 <sup>20</sup>	23 ±4	4	(1.6±0.6)·10 <sup>-11</sup>
2.0·10 <sup>20</sup>	40 ±4	6	(1.3±0.6)·10 <sup>-11</sup>
3.2·10 <sup>20</sup>	26 ±2	5	(1.6±0.6)·10 <sup>-11</sup>
4.1·10 <sup>20</sup>	19 ±1	5	(1.9±0.7)·10 <sup>-11</sup>
5.6·10 <sup>20</sup>	14 ±1	5	(1.9±0.7)·10 <sup>-11</sup>
7.3·10 <sup>20</sup>	11 ±1	4	(2.0±0.7)·10 <sup>-11</sup>
8.0·10 <sup>20</sup>	10 ±1	6	(2.4±0.8)·10 <sup>-11</sup>
9.0·10 <sup>20</sup>	9.7±0.7	6	(2.4±0.8)·10 <sup>-11</sup>
1.1·10 <sup>21</sup>	9.4±0.4	6	(2.2±0.8)·10 <sup>-11</sup>
1.3·10 <sup>21</sup>	6.7±1.0	5	(1.6±0.6)·10 <sup>-11</sup>
1.6·10 <sup>21</sup>	6.0±0.7	6	(1.7±0.6)·10 <sup>-11</sup>
1.8·10 <sup>21</sup>	4.0±1.0	4	(1.7±0.6)·10 <sup>-11</sup>
2.0·10 <sup>21</sup>	5.0±0.2	4	(1.9±0.7)·10 <sup>-11</sup>
2.3·10 <sup>21</sup>	10 ±1	2	(2.2±0.8)·10 <sup>-11</sup>
2.6·10 <sup>21</sup>	12 ±1	4	(2.5±0.9)·10 <sup>-11</sup>
3.0·10 <sup>21</sup>	12 ±1	4	(2.8±1.0)·10 <sup>-11</sup>
3.4·10 <sup>21</sup>	9.1±0.3	4	(3.0±1.0)·10 <sup>-11</sup>

mental uncertainty. Our experimental results on  $k_{1,\text{exp}}$  in He, therefore, can be combined with the results on  $k_{1,\text{exp}}$  from Refs. 11 and 12.

The combined representation of the present and the earlier results clearly gives a consistent picture in contrast to the analysis of Refs. 11 and 12 which led to values of  $k_1$  and  $k_9$  differing by a factor of 3. Only with the complete transition falloff curve of Fig. 5, the distinction between  $k_1$  and  $k_9$  can be made unambiguously. In order to do this, we employed a conventional falloff representation for  $k_1$  of the form

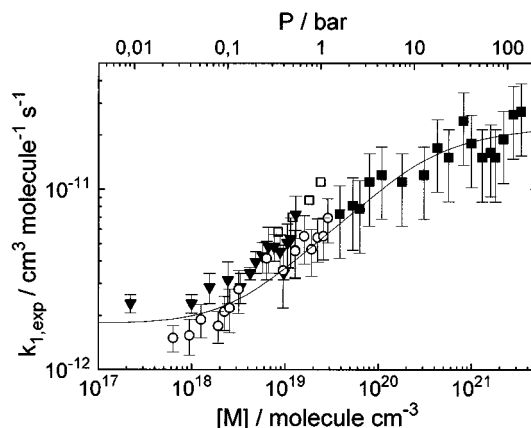


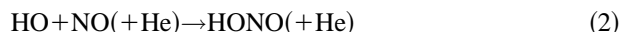
FIG. 5. Second-order rate constant  $k_{1,\text{exp}}$  for the reaction HO+HO (+M)→products at  $T=298 \text{ K}$  (■: M=He, this work, ○: M=N<sub>2</sub> (Ref. 12), ▼: M=N<sub>2</sub> (Ref. 11), □: M=SF<sub>6</sub> (Ref. 29), the solid line represents the fit with Eq. (22) and  $k_9 = 1.9 \times 10^{-12} \text{ cm}^3 \text{ molecule}^{-1} \text{ s}^{-1}$ ;  $k_{1,0} = 3.7 \times 10^{-31} [\text{He}] \text{ cm}^6 \text{ molecule}^{-2} \text{ s}^{-1}$ ;  $F_{1,\text{cent}} = 0.6$ , and  $k_{1,\infty} = 2.2 \times 10^{-11} \text{ cm}^3 \text{ molecule}^{-1} \text{ s}^{-1}$ ).

$$k_1 = \left[ \frac{k_{1,0}}{1 + k_{1,0}/k_{1,\infty}} \right] F_{1,\text{cent}}^{(1 + (\log(k_{1,0}/k_{1,\infty})/0.75 - 1.27 \log F_{1,\text{cent}})^2)^{-1}} \quad (22)$$

The falloff curve could well be fitted by choosing  $k_9 = 1.9 \times 10^{-12} \text{ cm}^3 \text{ molecule}^{-1} \text{ s}^{-1}$ ,  $k_{1,0} = 3.7 \times 10^{-31} [\text{He}] \text{ cm}^6 \text{ molecule}^{-2} \text{ s}^{-1}$ ,  $F_{1,\text{cent}} = 0.6$ , and  $k_{1,\infty} = 2.2 \times 10^{-11} \text{ cm}^3 \text{ molecule}^{-1} \text{ s}^{-1}$ . However, one should notice that the fitted limiting low pressure value of  $k_{1,0}$  strongly depends on the broadening factor  $F_{1,\text{cent}}$  and on  $k_9$ . An increase of 10% in the broadening factor causes a decrease of about 13% in  $k_{1,0}$  whereas  $k_{1,\infty}$  only slightly depends on  $F_{1,\text{cent}}$ . With the data from Ref. 29 we obtained  $k_{1,0} = 9.0 \times 10^{-31} [\text{SF}_6] \text{ cm}^6 \text{ molecule}^{-2} \text{ s}^{-1}$  and a broadening factor of  $F_{1,\text{cent}} = 0.8$  for the bath gas SF<sub>6</sub>. The  $k_{1,0}$  values from the present work differ strongly from the analysis of Ref. 12 and the corresponding recommendation of Ref. 4 which led to  $k_{1,0} = 6.0 \times 10^{-31} [\text{He}]$  and  $8.0 \times 10^{-31} [\text{N}_2] \text{ cm}^6 \text{ molecule}^{-2} \text{ s}^{-1}$  respectively. Clearly the present analysis based on data over a much wider pressure range is more reliable. It also removes the apparent discrepancy between the results of Refs. 11 and 12 which was claimed in Ref. 12. We estimate the combined statistical and evaluational errors of  $k_{1,0}$ ,  $k_{1,\infty}$ , and  $k_9$  to be  $\pm 20\%$  where a theoretical  $F_{1,\text{cent}}$  value of 0.6 is adopted from the analysis in Ref. 10.

### B. Falloff curve of the recombination reaction HO+NO(+He)→HONO(+He)

The reaction



was studied under pseudo-first-order conditions with initial values of the ratio  $[\text{HO}]_0/[\text{NO}]_0$  between  $10^{-2}$  and  $2 \times 10^{-2}$ . HO was generated via reactions (5) and (6) in gas mixtures containing H<sub>2</sub>O, N<sub>2</sub>O, NO (0.5–1.2 mbar), and He. The amount of NO additionally formed in reaction (14) could safely be neglected against the high initial concentration of NO. SLIF profiles of HO were fitted by a first-order rate law

$$[\text{HO}] = [\text{HO}]_0 \exp(-k_{2,\text{exp}} t) \quad (23)$$

The signals were fitted at times which were long enough for complete vibrational relaxation of HO. The first-order rate constant  $k_{2,\text{exp}}$  in Eq. (23) corresponds to the product of the pressure dependent second-order rate constant  $k_2$  of reaction (2) and the NO initial concentration  $[\text{NO}]_0$ .

The obtained second-order rate constants  $k_2$  are given in Table II; our results are compared in Fig. 6 with values from other groups.<sup>30–39</sup> Only experiments with the bath gas He are shown. One observes that, while there are only minor deviations from limiting low pressure behavior below 1 bar of He, the transition to a limiting high pressure range is practically achieved at 100 bar. There are discrepancies of a factor of 2 between the published low pressure rate constants. We adopt an average value of the low pressure limiting rate constant which is close to the value from Ref. 30 of  $k_{2,0} = 6.0 \times 10^{-31} [\text{He}] \text{ cm}^6 \text{ molecule}^{-2} \text{ s}^{-1}$ . The complete fall-off curve is then expressed by Eq. (22) using a high pressure limiting rate constant of  $k_{2,\infty} = 3.3 \times 10^{-11} \text{ cm}^3 \text{ molecule}^{-1} \text{ s}^{-1}$  and a theoretically calculated  $F_{2,\text{cent}} = 0.81$

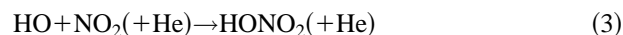
TABLE II. Second order rate constants for the reaction HO+NO (+He)→HONO(+He) ( $[\text{He}]$  in molecule  $\text{cm}^{-3}$ ,  $k_2$  in  $\text{cm}^3 \text{ molecule}^{-1} \text{ s}^{-1}$ , No.=number of experiments).

$[\text{He}]$	No.	$k_2$
$3.2 \cdot 10^{21}$	6	$(3.1 \pm 0.5) \cdot 10^{-11}$
$2.3 \cdot 10^{21}$	7	$(3.2 \pm 0.5) \cdot 10^{-11}$
$1.6 \cdot 10^{21}$	5	$(2.9 \pm 0.4) \cdot 10^{-11}$
$1.2 \cdot 10^{21}$	5	$(2.9 \pm 0.4) \cdot 10^{-11}$
$7.6 \cdot 10^{20}$	5	$(2.9 \pm 0.4) \cdot 10^{-11}$
$3.4 \cdot 10^{20}$	5	$(2.5 \pm 0.4) \cdot 10^{-11}$
$1.7 \cdot 10^{20}$	3	$(2.0 \pm 0.3) \cdot 10^{-11}$
$9.6 \cdot 10^{19}$	2	$(1.7 \pm 0.2) \cdot 10^{-11}$

from Ref. 4. The accuracy of the limiting high pressure rate constant is estimated to be  $\pm 20\%$ . A theoretical analysis of the rate constants will be given later together with results on the temperature dependence of  $k_{2,\infty}$  and the falloff curves.

### C. Falloff curve of the recombination reaction HO+NO<sub>2</sub>(+He)→HONO<sub>2</sub>(+He)

The experimental method for the determination of the rate constant for the reaction



differs slightly from the procedure described before. HO was produced via reaction (7) by photolyzing 0.4–2 mbar HNO<sub>3</sub> in the presence of 0.2–1 mbar of NO<sub>2</sub> in order to obtain an initial ratio of  $[\text{HO}]_0/[\text{NO}_2]_0$  near to  $5 \times 10^{-3}$ . Then again the pseudo-first-order decay of HO was monitored by SLIF. Total NO<sub>2</sub> partial pressures were limited to values below 1 mbar to prevent N<sub>2</sub>O<sub>4</sub> formation. At room temperature and these low partial pressures less than 5% of the NO<sub>2</sub> is bound as N<sub>2</sub>O<sub>4</sub>. The partial pressure of HNO<sub>3</sub> was kept below 2 mbar to prevent competition between the investigated recombination reaction (3) and the reaction

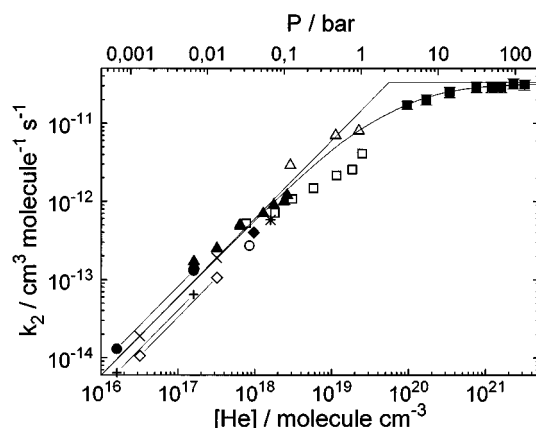


FIG. 6. Second-order rate constant  $k_2$  for the reaction HO+NO (+M)→HONO(+M) at  $T=298 \text{ K}$  with  $M=\text{He}$  (■: this work, □: Ref. 31, ▲: Ref. 32, ○: Ref. 33, △: Ref. 34, ◇: Ref. 35, ◆: Ref. 36, ●: Ref. 37, +: Ref. 38, ×: Ref. 30, \*: Ref. 39; the solid line represents the fit with Eq. (22) and  $k_{2,0} = 6.0 \times 10^{-31} [\text{He}] \text{ cm}^6 \text{ molecule}^{-2} \text{ s}^{-1}$ ,  $F_{2,\text{cent}} = 0.81$ , and  $k_{2,\infty} = 3.3 \times 10^{-11} \text{ cm}^3 \text{ molecule}^{-1} \text{ s}^{-1}$ ).

TABLE III. Second order rate constants for the reaction HO+NO<sub>2</sub>(+He)→HONO<sub>2</sub>(+He) ([He] in molecule cm<sup>-3</sup>,  $k_3$  in cm<sup>3</sup> molecule<sup>-1</sup> s<sup>-1</sup>, No.=number of experiments).

[He]	No.	$k_3$
3.6·10 <sup>21</sup>	5	(5.5±0.8)·10 <sup>-11</sup>
2.9·10 <sup>21</sup>	4	(5.4±0.8)·10 <sup>-11</sup>
1.9·10 <sup>21</sup>	4	(5.0±0.7)·10 <sup>-11</sup>
1.4·10 <sup>21</sup>	3	(4.9±0.7)·10 <sup>-11</sup>
9.5·10 <sup>20</sup>	12	(4.4±0.6)·10 <sup>-11</sup>
5.8·10 <sup>20</sup>	5	(4.1±0.7)·10 <sup>-11</sup>
4.0·10 <sup>20</sup>	10	(3.7±0.6)·10 <sup>-11</sup>
2.7·10 <sup>20</sup>	2	(3.3±0.6)·10 <sup>-11</sup>
2.5·10 <sup>20</sup>	2	(3.1±0.7)·10 <sup>-11</sup>
2.2·10 <sup>20</sup>	1	(3.0±0.6)·10 <sup>-11</sup>
1.5·10 <sup>20</sup>	4	(2.7±0.4)·10 <sup>-11</sup>
1.3·10 <sup>20</sup>	4	(2.2±0.3)·10 <sup>-11</sup>
1.1·10 <sup>20</sup>	4	(2.3±0.3)·10 <sup>-11</sup>
1.0·10 <sup>20</sup>	2	(2.2±0.3)·10 <sup>-11</sup>
8.9·10 <sup>19</sup>	7	(2.1±0.3)·10 <sup>-11</sup>
7.9·10 <sup>19</sup>	2	(1.9±0.4)·10 <sup>-11</sup>
6.4·10 <sup>19</sup>	9	(1.7±0.3)·10 <sup>-11</sup>
5.3·10 <sup>19</sup>	23	(1.6±0.3)·10 <sup>-11</sup>
4.5·10 <sup>19</sup>	5	(1.4±0.3)·10 <sup>-11</sup>
3.7·10 <sup>19</sup>	4	(1.3±0.2)·10 <sup>-11</sup>
2.5·10 <sup>19</sup>	3	(1.0±0.3)·10 <sup>-11</sup>
7.6·10 <sup>18</sup>	1	(3.5±2.0)·10 <sup>-12</sup>

for which  $k_{24}=1.5\times 10^{-13}$  cm<sup>3</sup> molecule<sup>-1</sup> s<sup>-1</sup>.<sup>4</sup>

Nitric acid is not very stable to heterogeneous decomposition such that decomposition on the walls of the high pressure stainless steel gas reservoir can lead to an increase of NO<sub>2</sub> concentrations. We checked this by photolyzing gas mixtures of 70 mbar HNO<sub>3</sub> and 40 bar He. HO loss in these experiments was only 4–5 times faster than expected for reaction (24). Since under our conditions the rate constant of reaction (3) is about 100 times larger than that of reaction (24), this indicates an additional partial pressure of NO<sub>2</sub> of less than 1 mbar. From this we conclude that in our reaction mixture the contribution from heterogeneous HNO<sub>3</sub> decomposition to the total NO<sub>2</sub> concentration could be neglected (<5%).

Table III shows the obtained rate constants for reaction (3). The data are plotted in Fig. 7 together with data from other groups<sup>30,35–37,40–45</sup> which have also used He as the bath gas. One observes a much broader falloff curve than in the case of the reaction HO+NO(+He)→HONO(+He) shown in Fig. 6. Near 100 bar of He one approaches the high pressure limit. While our experiments in bath gases different from He, which will be reported later, showed a smoother continuation of earlier results, with He a so far unexplained “irregularity” is observed between 0.1 and 1 bar. Although this is still within the error limits, our own relatively uncertain single experiment at 0.3 bar of He seems to confirm this anomaly. For the three parameter representation of the falloff curve of Eq. (22), we chose again the limiting low pressure rate constant  $k_{3,0}=1.6\times 10^{-30}$  [He] cm<sup>6</sup> molecule<sup>-2</sup> s<sup>-1</sup> from [30] which is in agreement with the recommendations from [4]. The limiting high pressure rate constant with a calculated  $F_{3,\text{cent}}=0.41$  from [4] then follows as  $k_{3,\infty}=7.5\times 10^{-11}$  cm<sup>3</sup> molecule<sup>-1</sup> s<sup>-1</sup>. The accuracy of  $k_{3,\infty}$  is estimated to

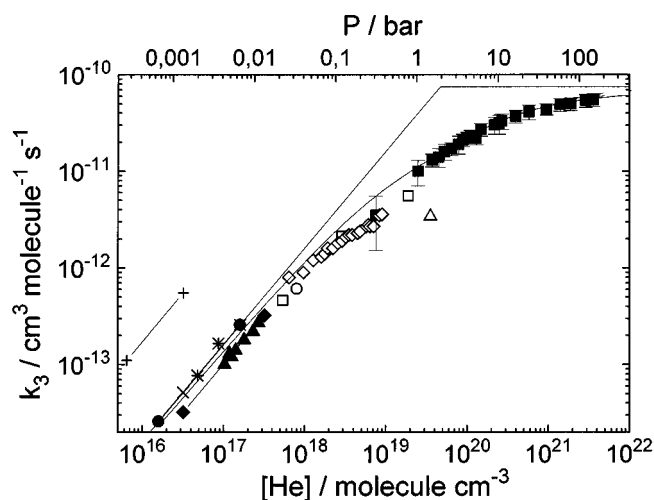
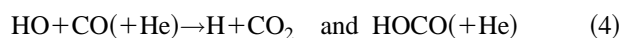


FIG. 7. Second-order rate constant  $k_3$  for the reaction HO+NO<sub>2</sub>(+M)→HONO<sub>2</sub>(+M) at  $T=298$  K with M=He (■: this work, □: Ref. 40, ▲: Ref. 41, ○: Ref. 42, △: Ref. 45, ◆: Ref. 35, ◇: Ref. 36, ●: Ref. 37, +: Ref. 44, -x-: Ref. 30, \*: Ref. 43; the solid line represents the fit with Eq. (22) and  $k_{3,0}=1.6\times 10^{-30}$  [He] cm<sup>6</sup> molecule<sup>-2</sup> s<sup>-1</sup>,  $F_{3,\text{cent}}=0.41$ , and  $k_{3,\infty}=7.5\times 10^{-11}$  cm<sup>3</sup> molecule<sup>-1</sup> s<sup>-1</sup>).

±20%. Clearly, this falloff representation does not account for the S-shaped rate constant anomaly between 0.1 and 1 bar of He which has to be reconfirmed and which was not observed in other bath gases. A theoretical analysis of the rate constants will be given later together with results on the temperature dependence of  $k_{3,\infty}$ .

#### D. Pressure dependence of the reaction HO+CO(+He)→H+CO<sub>2</sub> and HOCO(+He)

We studied the reaction



under pseudo-first order conditions with initial values of the ratio  $[\text{HO}]_0/[\text{CO}]_0$  near to  $5\times 10^{-3}$ . Again HO was produced via reactions (5) and (6) in mixtures containing H<sub>2</sub>O, N<sub>2</sub>O, 50–200 mbar of CO, and the bath gas He. SLIF profiles were fitted by a first-order rate law for HO decay, starting at times large enough for complete vibrational relaxation of HO. Table IV summarizes our results, which are also dis-

TABLE IV. Second order rate constants for the reaction HO+CO(+He)→H+CO<sub>2</sub> and HOCO(+He) ([He] in molecule cm<sup>-3</sup>,  $k_4$  in cm<sup>3</sup> molecule<sup>-1</sup> s<sup>-1</sup>, No.=number of experiments).

[He]	No.	$k_4$
3.0·10 <sup>21</sup>	7	(8.1±1.2)·10 <sup>-13</sup>
1.8·10 <sup>21</sup>	8	(7.3±1.2)·10 <sup>-13</sup>
1.3·10 <sup>21</sup>	2	(7.0±1.1)·10 <sup>-13</sup>
8.5·10 <sup>20</sup>	2	(6.1±0.9)·10 <sup>-13</sup>
4.8·10 <sup>20</sup>	3	(5.6±0.9)·10 <sup>-13</sup>
2.3·10 <sup>20</sup>	9	(4.5±0.7)·10 <sup>-13</sup>
1.7·10 <sup>20</sup>	14	(3.8±0.6)·10 <sup>-13</sup>
1.2·10 <sup>20</sup>	9	(3.4±0.5)·10 <sup>-13</sup>
8.4·10 <sup>19</sup>	3	(3.0±0.5)·10 <sup>-13</sup>
4.2·10 <sup>19</sup>	3	(2.4±0.4)·10 <sup>-13</sup>
3.4·10 <sup>19</sup>	2	(2.2±0.3)·10 <sup>-13</sup>

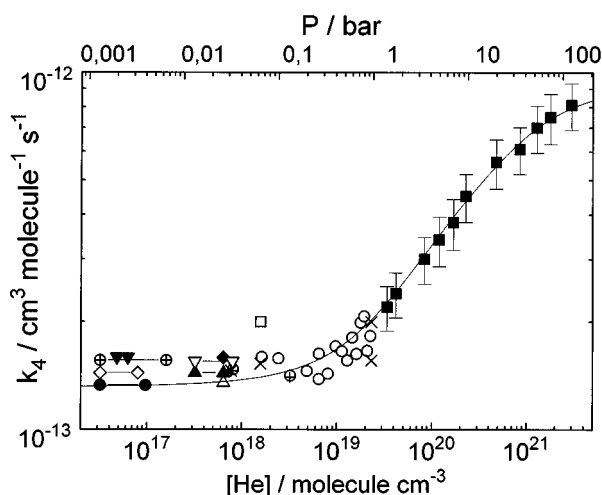
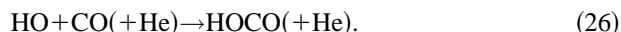
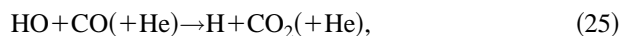


FIG. 8. Second-order rate constant  $k_4$  for the reaction  $\text{HO}+\text{CO}(+\text{M})\rightarrow\text{H}+\text{CO}_2$  and  $\text{HOCO}(+\text{M})$  at  $T=298$  K with  $\text{M}=\text{He}$  [■: this work, □: Ref. 52, -▲: Ref. 48, ○: Ref. 56, △: Ref. 46, -◇: Ref. 47, -◆: Ref. 50, -●: Ref. 49, +: Ref. 53, ×: Ref. 54, -▽: Ref. 51, \*: Ref. 57, -▼: Ref. 55, -⊕: Ref. 38; the solid line represents the fit with Eqs. (27)–(33)].

played in Fig. 8 in comparison with data from other groups,<sup>38,46–57</sup> as far as they have also used the bath gas He.

Figure 8 demonstrates a marked increase of the apparent second-order rate constant with increasing pressure above 1 bar. The only weak pressure dependence below 1 bar, which for a long time was overlooked before it became well established, is continued over a wide range in our experiments and is clearly confirmed. Obviously, only with measurements above 1 bar a complete picture emerges which again confirms the necessity of high pressure measurements.

Figure 8 shows a similar S-shaped transition curve between a limiting low pressure and high pressure rate constant as observed in Fig. 5 for the self-reaction of HO radicals. The question arises whether two separable reaction channels, like reactions (1) and (9) for the HO self-reaction, contribute or whether a complex-forming bimolecular reaction with a common intermediate is present.<sup>48,58</sup> From *ab initio* calculations<sup>59</sup> one concludes that the HOCO radical, highly excited and possibly in various isomeric forms, is the common intermediate for the two reaction steps.



The inclusion of He in reaction (25) indicates that collisions may modify the energy and angular momentum distribution of HOCO\* before it reacts to  $\text{H}+\text{CO}_2$ . The detailed theoretical analysis of reactions (25) and (26), in terms of RRKM theory and a master equation, will be presented later together with measurements over extended temperature ranges.<sup>13</sup> From this analysis, a simplified expression of the rate constant for HO consumption is derived in the form

$$k_4=k_{25}+k_{26}, \quad (27)$$

with

TABLE V. Comparison of high pressure recombination, isotope exchange, and vibrational relaxation rate constants ( $k$  in  $\text{cm}^3 \text{ molecule}^{-1} \text{ s}^{-1}$ ).

Reaction	$k$	Method	Ref.
HO+NO	$1.8 \cdot 10^{-11}$	Recombination	31
	$8.5 \cdot 10^{-12}$	Recombination	32
	$8.5 \cdot 10^{-12}$	Recombination	33
	$1.2 \cdot 10^{-11}$	Recombination	34
	$>8.0 \cdot 10^{-12}$	Recombination	64
	$(3.3 \pm 0.6) \cdot 10^{-11}$	Recombination	This work
	$(\geq 3.6 \pm 1.2) \cdot 10^{-11}$	Isotope exchange	47
	$(\geq 4.2 \pm 1.0) \cdot 10^{-11}$	Isotope exchange	63
	$(3.8 \pm 0.6) \cdot 10^{-11}$	Vibrational relaxation	28
	$(1.5 \pm 0.4) \cdot 10^{-11}$	Vibrational relaxation	65
	$6 \cdot 10^{-11}$	Vibrational relaxation	66
HO+NO <sub>2</sub>	$>1.6 \cdot 10^{-11}$	Recombination	40
	$1.6 \cdot 10^{-11}$	Recombination	42
	$5.2 \cdot 10^{-12}$	Recombination	67
	$>3.0 \cdot 10^{-11}$	Recombination	68
	$(7.5 \pm 1.5) \cdot 10^{-11}$	Recombination	This work
	$(\geq 1.5 \pm 0.6) \cdot 10^{-11}$	Isotope exchange	47
	$(1.1 \pm 0.2) \cdot 10^{-11}$	Isotope exchange	63
	$(4.8 \pm 0.8) \cdot 10^{-11}$	Vibrational relaxation	28
HO+CO	$(1.3 \pm 0.3) \cdot 10^{-11}$	Vibrational relaxation	65
	$<k_{\text{relax.}}(\text{HO}+\text{NO})$	Vibrational relaxation	66
	$3.6 \cdot 10^{-13}$	Recombination	34
	$(9.7 \pm 1.9) \cdot 10^{-13}$	Recombination	This work
	$<3 \cdot 10^{-13}$	Vibrational relaxation	69
	$(10 \pm 2) \cdot 10^{-13}$	Vibrational relaxation	62

$$k_{25} \approx k_{25,0} \left[ 1 - \frac{x}{1+x} F_{4,\text{cent}}^{[1+(\log x)^2]^{-1}} \right], \quad (28)$$

$$k_{26} \approx k_{26,0} \left[ \frac{1+xy}{1+x} \right] F_{4,\text{cent}}^{[1+(\log x)^2]^{-1}}, \quad (29)$$

$$x = k_{26,0} / (k_{26,\infty} - k_{25,0}) \quad \text{and} \quad xy = k_{25,0} / k_{26,\infty}, \quad (30)$$

where  $F_{4,\text{cent}}$  is a center broadening factor for the two-channel thermal dissociation of HOCO into  $\text{HO}+\text{CO}$  and  $\text{H}+\text{CO}_2$ . This form of  $k_4$  well represents the data of Fig. 8 where the following limiting rate constants are fitted:

$$k_{25,0} = 1.3 \times 10^{-13} \text{ cm}^3 \text{ molecule}^{-1} \text{ s}^{-1} \quad (31)$$

on the basis of the data from Refs. 13 and 49,

$$k_{26,0} = 4.1 \times 10^{-33} [\text{He}] \text{ cm}^6 \text{ molecule}^{-2} \text{ s}^{-1} \quad (32)$$

and

$$k_{26,\infty} = 9.7 \times 10^{-13} \text{ cm}^3 \text{ molecule}^{-1} \text{ s}^{-1}. \quad (33)$$

A center broadening factor  $F_{4,\text{cent}}=0.69$  was taken from the theoretical analysis of Ref. 13. The accuracy of the values of  $k_{26,0}$  and  $k_{26,\infty}$  is estimated to be  $\pm 20\%$ . Equations (25)–(33) well represent the transition falloff curve of Fig. 8; in addition, they indicate how much HOCO is formed in comparison to  $\text{HO}+\text{CO}$  at a given pressure of the bath gas He and at 298 K. This quantity sensitively depends on the nature of the bath gas, see Ref. 13.

## V. COMPARISON OF LIMITING HIGH PRESSURE RATE CONSTANTS WITH VIBRATIONAL RELAXATION AND ISOTOPE EXCHANGE DATA

Limiting high pressure rate constants for radical–radical recombination reactions are known to be closely related to rate constants for vibrational relaxation and isotope exchange processes, provided that the same intermediate complexes are involved.<sup>60,61</sup> Therefore, a comparison of our results with the corresponding data appears obligatory. Table V gives a summary. In any case, the high pressure recombination rate constant, i.e., the rate constant for capture provides an upper limit for vibrational relaxation and isotope exchange, because in the latter processes backdissociation into the entrance channels takes place. In vibrational relaxation, the importance of this backdissociation increases with increasing temperature. A quantitative analysis of this effect for the HO+CO system is given in Ref. 13.

For the HO+CO system, indeed the present high pressure rate constants and vibrational relaxation rate constants near room temperature from Ref. 62 perfectly agree. Earlier results appear in error. The same is true for the HO+NO system. Again the last measurements of vibrational relaxation<sup>28</sup> and isotope exchange rate constants<sup>47,63</sup> agree very well with the high pressure recombination rate constant from the present work while earlier results often were erroneous. The situation appears less well characterized for the HO+NO<sub>2</sub> system. The last measurements of the vibrational relaxation rate constants<sup>28,65</sup> are still somewhat below but close to the high pressure recombination rate constant. However, isotope exchange rates are much slower.<sup>47,63</sup> Whether this is an experimental artifact or real, remains to be clarified.

In summary, vibrational relaxation (and to some extent isotope exchange) through complex-forming bimolecular reactions are complementary to high pressure recombination although they are not the same. This aspect will be elaborated theoretically in Ref. 13.

## ACKNOWLEDGMENTS

Financial support of this work by the Deutsche Forschungsgemeinschaft (SFB 357 *Molekulare Mechanismen Unimolekularer Reaktionen*) is gratefully acknowledged.

- <sup>1</sup>J. Troe, *J. Phys. Chem.* **90**, 3485 (1986).
- <sup>2</sup>J. Troe, *Ber. Bunsenges. Phys. Chem.* **92**, 242 (1988).
- <sup>3</sup>J. Troe, *Z. Phys. Chem. NF* **161**, 209 (1989).
- <sup>4</sup>R. Atkinson, D. L. Baulch, R. A. Cox, R. F. Hampson, J. A. Kerr, and J. Troe, *J. Phys. Chem. Ref. Data* **21**, 1125 (1992).
- <sup>5</sup>D. L. Baulch, C. J. Cobos, R. A. Cox, C. Esser, P. Frank, Th. Just, J. A. Kerr, M. J. Pilling, J. Troe, R. W. Walker, and J. Warnatz, *J. Phys. Chem. Ref. Data* **21**, 411 (1992).
- <sup>6</sup>A. E. Croce de Cobos, H. Hippler, and J. Troe, *J. Phys. Chem.* **88**, 5083 (1984).
- <sup>7</sup>H. Hippler, K. Luther, A. R. Ravishankara, and J. Troe, *Z. Phys. Chem. NF* **142**, 1 (1984).
- <sup>8</sup>C. J. Cobos, H. Hippler, and J. Troe, *J. Phys. Chem.* **89**, 342 (1985).
- <sup>9</sup>R. Atkinson, *J. Phys. Chem. Ref. Data, Monograph No. 1* (1989).
- <sup>10</sup>L. Brouwer, C. J. Cobos, J. Troe, H.-R. Dübal, and F. F. Crim, *J. Chem. Phys.* **86**, 6171 (1987).
- <sup>11</sup>D. W. Trainor and C. W. von Rosenberg, *J. Chem. Phys.* **61**, 1010 (1974).
- <sup>12</sup>R. Zellner, F. Ewig, R. Paschke, and G. Wagner, *J. Phys. Chem.* **92**, 4184 (1988).
- <sup>13</sup>D. Fulle, H. F. Hamann, H. Hippler, and J. Troe, *J. Chem. Phys.* (to be published).
- <sup>14</sup>E. H. Piepmeier, *Spectrochim. Acta B* **27**, 431 (1972); J. W. Daily, *Appl. Opt.* **6**, 568 (1977).
- <sup>15</sup>J. B. Jeffries, G. P. Smith, D. E. Heard, and D. R. Crosely, *Ber. Bunsenges. Phys. Chem.* **96**, 1411 (1992).
- <sup>16</sup>A. C. Eckbreth in *Laser Diagnostics for Combustion, Temperature, and Species*, edited by A. K. Gupta and D. G. Lilley (Abacus, Mass., 1988).
- <sup>17</sup>A. Jörg, U. Meier, and K. Kohse-Höinghaus, *J. Chem. Phys.* **93**, 6453 (1990); R. Kienle, PhD. thesis, Universität Bielefeld, Germany, 1994.
- <sup>18</sup>I. J. Wysong, J. B. Jeffries, and D. R. Crosely, *J. Chem. Phys.* **93**, 6453 (1990).
- <sup>19</sup>J. Schleipen, PhD. thesis, University of Nijmegen, Netherland, 1992; J. Schleipen, A. Eppink, and J. J. ter Meulen (to be published).
- <sup>20</sup>C. C. Wang and C. M. Huang, *Phys. Rev. A* **21**, 1235 (1980).
- <sup>21</sup>G. Ortgies, PhD. thesis, Universität Frankfurt, Germany, 1982; W. Armeding, A. Herbert, T. Schindler, M. Spiekermann, and F. J. Comes, *Ber. Bunsenges. Phys. Chem.* **94**, 776 (1980).
- <sup>22</sup>G. P. Glass, H. Endo, and B. K. Chaturvedi, *J. Chem. Phys.* **77**, 5450 (1982); R. K. Lengel, and D. R. Crosely, *J. Chem. Phys.* **68**, 5309 (1978); K. R. Rensberger, J. B. Jeffries, and D. R. Crosely, *J. Chem. Phys.* **90**, 2174 (1989).
- <sup>23</sup>C. W. Gear, *Numerical Initial Value Problems in Ordinary Differential Equations* (Prentice-Hall, New York, 1971).
- <sup>24</sup>L. B. Harding, *J. Phys. Chem.* **93**, 8004 (1984); **95**, 8653 (1991).
- <sup>25</sup>L. B. Harding and A. F. Wagner, 22nd Int. Symp. on Combustion (The Combustion Institute, Pittsburgh, 1988), p. 983.
- <sup>26</sup>H. Hippler, R. Rahn, and J. Troe, *J. Chem. Phys.* **93**, 6560 (1990).
- <sup>27</sup>K. H. Gericke and F. J. Comes, *Chem. Phys. Lett.* **81**, 218 (1981).
- <sup>28</sup>I. W. M. Smith and M. D. Williams, *J. Chem. Soc. Faraday Trans. 2* **81**, 1849 (1985).
- <sup>29</sup>K. Fagerström, A. Lund, G. Mahmoud, J. T. Jodkowski, and E. Ratajczak, *Chem. Phys. Lett.* **224**, 43 (1994).
- <sup>30</sup>J. P. Burrows, T. J. Wallington, and R. P. Wayne, *J. Chem. Soc. Faraday Trans. 2* **79**, 111 (1983).
- <sup>31</sup>R. Overend, G. Paraskevopoulos, and C. Black, *J. Chem. Phys.* **64**, 4149 (1976).
- <sup>32</sup>F. Stuhl and H. Niki, *J. Chem. Phys.* **57**, 3677 (1972).
- <sup>33</sup>C. Anastasi and I. W. M. Smith, *J. Chem. Soc. Faraday Trans. 2* **74**, 1056 (1978).
- <sup>34</sup>B. K. T. Sie, R. Simonaitis, and J. Hecklen, *Int. J. Chem. Kinet.* **8**, 99 (1976).
- <sup>35</sup>J. G. Anderson, J. J. Margitan, and F. Kaufman, *J. Chem. Phys.* **60**, 3310 (1974).
- <sup>36</sup>C. Morley and I. W. M. Smith, *J. Chem. Soc. Faraday Trans. 2* **68**, 1016 (1972).
- <sup>37</sup>A. A. Westenberg and N. DeHaas, *J. Chem. Phys.* **57**, 5375 (1972).
- <sup>38</sup>C. J. Howard and K. M. Evenson, *J. Chem. Phys.* **61**, 1943 (1974).
- <sup>39</sup>E. R. Lovejoy, T. P. Murrells, A. R. Ravishankara, and C. J. Howard, *J. Phys. Chem.* **94**, 2386 (1990).
- <sup>40</sup>P. H. Wine, N. M. Kreutter, and A. R. Ravishankara, *J. Phys. Chem.* **83**, 3191 (1979).
- <sup>41</sup>K. Erler, D. Field, R. Zellner, and I. W. M. Smith, *Ber. Bunsenges. Phys. Chem.* **81**, 22 (1977); K. Erler, D. Field, U. Welzbacher, and R. Zellner, *ibid.* **80**, 1226 (1976).
- <sup>42</sup>C. Anastasi and I. W. M. Smith, *J. Chem. Soc. Faraday Trans. 2* **72**, 1459 (1976).
- <sup>43</sup>L. G. Anderson, *J. Phys. Chem.* **84**, 2152 (1980).
- <sup>44</sup>M. F. R. Mulcahy and R. H. Smith, *J. Chem. Phys.* **54**, 5215 (1971).
- <sup>45</sup>E. Simonaitis and J. Hecklen, *Int. J. Chem. Kinet.* **4**, 529 (1972).
- <sup>46</sup>F. Stuhl and H. Niki, *J. Chem. Phys.* **57**, 3671 (1972).
- <sup>47</sup>G. D. Greenblatt and C. J. Howard, *J. Phys. Chem.* **93**, 1035 (1989).
- <sup>48</sup>I. W. M. Smith and R. Zellner, *J. Chem. Soc. Faraday Trans. 2* **69**, 1617 (1973).
- <sup>49</sup>A. A. Westenberg and N. DeHaas, *J. Chem. Phys.* **58**, 4061 (1973).
- <sup>50</sup>P. D. Davis, S. Fischer, and R. Schiff, *J. Chem. Phys.* **61**, 2213 (1974).
- <sup>51</sup>W. Steinert and R. Zellner, *Deuxième Symp. Eur. Comb.* **2**, 31 (1975).
- <sup>52</sup>R. Overend and G. Paraskevopoulos, *Chem. Phys. Lett.* **49**, 109 (1977).
- <sup>53</sup>N. R. Greiner, *J. Chem. Phys.* **51**, 5049 (1969).
- <sup>54</sup>H. W. Biermann, C. Zetzsch, and F. Stuhl, *Ber. Bunsenges. Phys. Chem.* **82**, 633 (1978).
- <sup>55</sup>M. A. A. Clyne and P. M. Holt, *J. Chem. Soc. Faraday Trans. 2* **75**, 569 (1979).
- <sup>56</sup>G. Paraskevopoulos and R. S. Irwin, *J. Chem. Phys.* **80**, 259 (1984).

- <sup>57</sup>D. Husain, J. M. C. Plane, and N. K. H. Slater, *J. Chem. Soc. Faraday Trans. 2* **77**, 1949 (1981).
- <sup>58</sup>J. Troe, *J. Chem. Soc. Faraday Trans.* **90**, 2303 (1994).
- <sup>59</sup>K. Kudla, G. C. Schatz, and A. F. Wagner, *J. Chem. Phys.* **95**, 1635 (1991).
- <sup>60</sup>R. P. Fernando and I. W. M. Smith, *Chem. Phys. Lett.* **66**, 218 (1979); *J. Chem. Soc. Faraday Trans 2* **77**, 459 (1981).
- <sup>61</sup>M. Quack and J. Troe, *Ber. Bunsenges. Phys. Chem.* **79**, 170 (1975); **81**, 160 (1975); M. Quack, *J. Phys. Chem.* **83**, 150 (1979).
- <sup>62</sup>J. Brunning, D. W. Derbyshire, I. W. M. Smith, and M. D. Williams, *J. Chem. Soc. Faraday Trans. 2* **84**, 105 (1988).
- <sup>63</sup>P. Dransfeld, J. Lukacs, and H. Gg. Wagner, *Z. Naturforsch. Teil A* **41**, 1283 (1986).
- <sup>64</sup>R. Atkinson, D. A. Hanson, and J. N. Pitts, *J. Chem. Phys.* **62**, 3284 (1975).
- <sup>65</sup>D. H. Jaffer and I. W. M. Smith, *Faraday Discuss. Chem. Soc.* **67**, 212 (1979).
- <sup>66</sup>J. E. Spencer and G. P. Glass, *Chem. Phys.* **15**, 35 (1976).
- <sup>67</sup>K. Glänzer and J. Troe, *Ber. Bunsenges. Phys. Chem.* **78**, 71 (1971).
- <sup>68</sup>J. S. Robertsshaw and I. W. M. Smith, *J. Phys. Chem.* **86**, 785 (1982).
- <sup>69</sup>J. E. Spencer, H. Endo, and G. P. Glass, 16th Symp. (Int.) on Comb. (The Combustion Institute, Pittsburgh, 1977), p. 829.